

Contents lists available at [ScienceDirect](https://www.sciencedirect.com)

# Case Studies in Construction Materials

journal homepage: [www.elsevier.com/locate/cscm](http://www.elsevier.com/locate/cscm)

## Reliability-based design method for shear capacity of steel reinforced engineered cementitious composites (ECC) beams

Qiao Liao<sup>a,b</sup>, Jiang-Tao Yu<sup>a</sup>, Yuan-Rui Su<sup>a</sup>, Wen-Guang Chen<sup>a,\*</sup>

<sup>a</sup> College of Civil Engineering, Tongji University, Shanghai 200092, China

<sup>b</sup> Department of Civil and Environmental Engineering, The Hong Kong Polytechnic University, Hung Hom, Kowloon, Hong Kong, China

### ARTICLE INFO

#### Keywords:

Engineered cementitious composites  
Monte Carlo simulation  
Shear capacity  
Reliability analysis

### ABSTRACT

Engineered cementitious composites (ECC) is famous for its excellent tensile deformability and crack width control ability. Steel reinforced ECC beams under shear loading exhibit brittle behaviors, which leads to a lack of structural safety. The reliability-based shear capacity model of steel reinforced ECC beams needs to be established for ensuring the structural shear safety. In this research, a test database of steel reinforced ECC beams under shear loading was constructed based on the given selecting principles. Through considering the shear resistance provided by fibers, the shear capacity model of steel reinforced ECC beams was preliminary established. The statistical characteristics of random variables were described and determined, and reliability index was calculated through Monte Carlo simulation. It is found that reliability index increases with increasing ECC strength, while decreases with increasing stirrup strength or stirrup ratio, especially at the high partial factor of ECC. For different target reliability indexes, the recommended partial factors of ECC are obtained through calibration. This research supplies a useful reference for the shear design of steel reinforced ECC beams in the actual engineering.

### 1. Introduction

The brittle nature of Portland cementitious concrete always results in some inferior performances in reinforced concrete (RC) structures, such as excessive crack width in service life or catastrophic failure at ultimate limited state. Engineered cementitious composites (ECC) is an emerging class of high-performance fiber reinforced concrete (FRC), and it is specially developed for overcoming the brittleness of Portland cementitious concrete [1–3]. ECC reinforced by polypropylene (PP) or polyvinyl alcohol (PVA) fibers possesses a tensile strain capacity of over 2% [4–8], and the corresponding average crack width is around 60 μm before fracture [9]. Particularly, the tensile strain capacity of ECC reinforced by polyethylene (PE) fibers is over 6% [10–18], exhibiting the similar deformability as the steel bars used to reinforce concrete [19].

ECC material has excellent mechanical properties [4–18,20], which prompts many researchers to investigate the mechanical performance of ECC members. In particular, the shear behaviors of ECC beams reinforced by steel bars have been extensively researched in recent decades [21–31]. The shear behaviors of steel reinforced ECC beams with different stirrup ratios were investigated in the literature [21]. For beams without stirrup, the shear capacity of ECC beams were observed to be about twice that of RC beams. When a stirrup ratio of 0.42% was adopted, the shear capacity of ECC beams increased by 20.56% in comparison with RC beams. Similarly, the shear capacity of ECC beams without stirrup was 170% that of RC beams [26]. As stirrup ratio was 0.38%, the shear

\* Corresponding author.

E-mail address: [wenguang\\_chen@tongji.edu.cn](mailto:wenguang_chen@tongji.edu.cn) (W.-G. Chen).

<https://doi.org/10.1016/j.cscm.2023.e02681>

Received 6 October 2023; Received in revised form 10 November 2023; Accepted 13 November 2023

Available online 14 November 2023

2214-5095/© 2023 The Author(s). Published by Elsevier Ltd. This is an open access article under the CC BY-NC-ND license (<http://creativecommons.org/licenses/by-nc-nd/4.0/>).

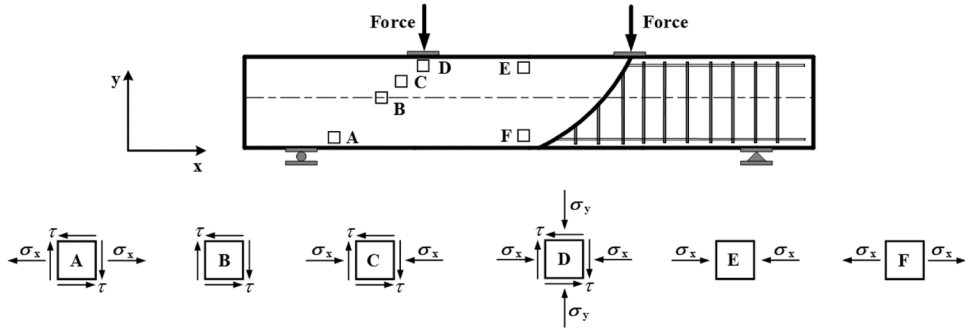


Fig. 1. Stress states of ECC material in beam [18,19].

capacity of ECC beams increased by only 13 % when compared with RC beams. The main reason for above results is the partial yielding of stirrups at peak load. Besides, Xu et al. [25] studied the shear behaviors of ECC beams with different shear-span ratios and longitudinal reinforcement ratios. Maximum shear crack width was within 100  $\mu\text{m}$  at serviceability state. ECC beams showed more ductile shear failure (i.e. many micro shear cracks) in comparison with RC beams, which results from the bridging effect of fibers [27]. Generally, steel reinforced ECC beams exhibit high shear capacity, tight crack width and satisfactory ductility. As shown in Fig. 1, ECC under uniaxial tension (point F) shows tensile strain-hardening accompanied with many micro-cracks [4]. Additionally, ECC under tension-shear loading (point A) displays displacement-hardening and outstanding crack width control [18]. ECC under compression-shear loading (point C) displays more ductile failure mode when compared with mortar [20]. Currently, many experimental studies have been conducted on the shear performance of steel reinforced ECC beams, but there is limited research on shear capacity model.

As mentioned above, steel reinforced ECC beams have high shear capacity in comparison with RC beams. Researchers make great efforts to establish shear capacity model, which aims to serve engineering applications. Based on ACI 318-14 and EN 1992-1-1:2004, a shear capacity model for steel reinforced ECC beams was established in the literature [24]. The predicted results agreed well with the test results of beams with various shear-span ratios, stirrup ratios and longitudinal reinforcement ratios. Additionally, the shear capacity model of steel reinforced ECC beams was established in the literature [32], which was stemmed from the modified compression field theory. The mean value and coefficient of variation (COV) of test results to predicted results (i.e. model error) were 1.05 and 0.197, respectively. However, the number of ECC beams used to validate shear capacity model was limited in the literature [24,32]. The shear capacity models in the literature [24,32] are relatively complex, which is not conducive to being mastered by designers. More importantly, the shear mechanisms of ECC beams are less well-understood, which may result in the high COV of model error. To simplify shear capacity model and guarantee structural safety, the simplified and reliability-based shear capacity model of steel reinforced ECC beams needs to be established.

In the present study, according to the given selecting principles, a test database of steel reinforced ECC beams under shear loading is constructed. According to GB 50010-2010 [33] and considering the shear resistance provided by PP or PVA fibers, the simplified shear capacity model of steel reinforced ECC beams is preliminary established. The statistical characteristics related to random variables are described and calculated. Reliability index is calculated by Monte Carlo simulation. Further, the recommended partial factors corresponding to various target reliability indexes are acquired through calibration.

**2. Test database**

A solid test database is critical for the reliability analysis of shear capacity of steel reinforced ECC beams [34]. In this research, the screening principles of test database are as follows. (1) Data with diagonal compression failure, diagonal tension failure and flexure failure is eliminated. (2) Data that does not describe material properties, especially the ultimate tensile strength of ECC, is removed. Accordingly, a detailed test database of steel reinforced ECC beams under shear loading was constructed. Table A in Appendix A lists the details of the test database. The established database included 64 test data [21-31], which is from 2004 to 2022. It is noteworthy that ECC in these beams is reinforced by PP or PVA fibers. Each beam in the test database includes dimensions (i.e. cross section and shear-span ratio), material properties (i.e. ECC and steel bars) and test results (i.e. shear capacity).

**3. Shear capacity model of steel reinforced ECC beams**

To apply the established shear capacity model in China, this shear capacity model will be mainly based on GB 50010-2010 [33] rather than other codes. According to GB 50010-2010 [33], the shear capacity of RC beams is expressed as

$$V_u = 0.7f_tbh_0 + f_{yv} \frac{A_{sv}}{s} h_0 \tag{1}$$

where  $f_t$  is the ultimate tensile strength of concrete (or ECC).  $b$  is the width of cross section.  $h_0$  is the effective height of cross section.  $f_{yv}$

**Table 1**  
Statistical parameters of model error.

Reduction coefficient $\eta$	Model error $\mu$		
	Mean value	Standard deviation	Coefficient of variation
1.0	0.71	0.25	0.36
0.9	0.75	0.27	0.36
0.8	0.79	0.28	0.35
0.7	0.84	0.29	0.35
0.6	0.89	0.31	0.35
0.5	0.95	0.33	0.35
0.4	1.02	0.35	0.34
0.3	1.10	0.37	0.34
0.2	1.20	0.40	0.34
0.1	1.32	0.44	0.33

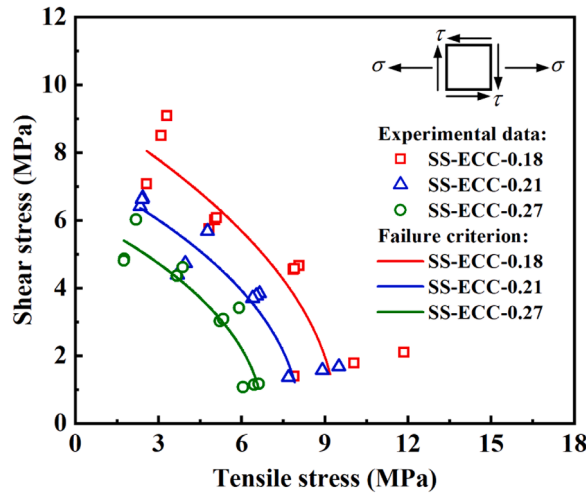


Fig. 2. Failure criterion of ECC subjected to tension-shear loading [18].

is the yield strength of steel stirrups.  $A_{sv}$  is the cross-section area of steel stirrups.  $s$  is the stirrup space. It is noteworthy that  $0.7f_tbh_0$  in Eq. (1) is the shear resistance supplied by the compression-shear zone concrete of beam, and  $f_{yv}\frac{A_{sv}}{s}h_0$  is the shear resistance mainly supplied by steel stirrups.

ECC possesses high tension-shear strength (point A in Fig. 1), shear strength (point B) and compression-shear strength (point C) in comparison with concrete [18,20,35]. More importantly, ECC under combined tension and shear is able to supply resistance after cracking [18]. Therefore, Eq. (1) cannot be applied for predicting the shear capacity of steel reinforced ECC beams.

To accurately predict shear capacity, it is necessary to consider the shear resistance supplied by fibers (i.e. tension-shear zone ECC of beam). According to JSCE recommendations [36], the shear resistance supplied by fibers can be acquired by

$$V_{\text{fiber}} = \frac{f_t b z}{\tan \beta} \tag{2}$$

where  $z$  is the distance between the action point of compression zone and the center point of tensile steel bars, usually taken as  $z = h_0/1.15$ .  $\beta$  is the inclined angle of the critical shear crack, usually taken as  $\beta = 45^\circ$ . Actually, Eq. (2) describes the shear contribution supplied by fibers on the oblique section of ECC beams. Therefore, the shear capacity of steel reinforced ECC beams can be expressed as

$$V_u = 0.7f_t b h_0 + f_{yv} \frac{A_{sv}}{s} h_0 + \frac{f_t b z}{\tan \beta} \tag{3}$$

To validate the accuracy and effectiveness of the shear capacity model, the predicted results  $V_{up}$  are compared with the experimental results  $V_{uc}$  listed in test database. Model error  $\mu$  is the ratio of the experimental results to the predicted results, namely  $\mu = V_{uc}/V_{up}$ . Table 1 lists the statistical parameters of model error. It is observed that the mean value of model error is about 0.71. Obviously, the predicted results are greater in comparison with the test results, which results from the decreasing of the tensile stress because of the existence of shear stress (Fig. 2) and stirrups. Concrete material under tension-shear loading exhibits a similar result [37]. To accurately predict shear capacity, the shear contribution provided by fibers should be calibrated [21].

Therefore, reduction coefficient  $\eta$  is introduced into Eq. (3) for a better prediction. The shear capacity of steel reinforced ECC beams

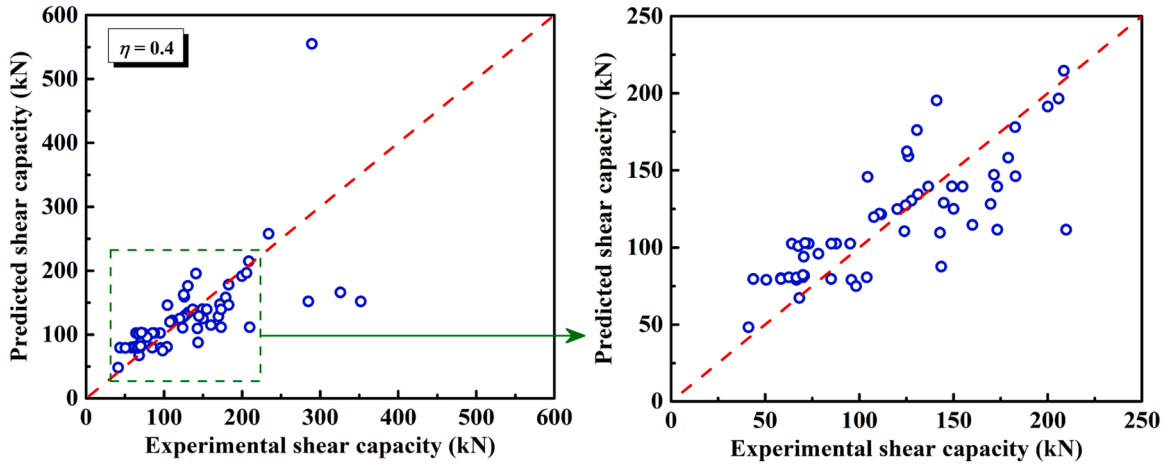


Fig. 3. Relationship between the predicted shear capacity and the experimental shear capacity.

**Table 2**  
Statistical parameters and distribution types of load.

Load type	Bias	Coefficient of variation	Distribution type	Reference
Dead load	1.060	0.070	Normal distribution	[39]
House live load	0.644	0.233	Extreme type I distribution	[39]
Office live load	0.524	0.288	Extreme type I distribution	[39]

Note: Bias is the ratio of mean value to standard value.

can be expressed as

$$V_u = 0.7f_t b h_0 + f_{yv} \frac{A_{sv}}{s} h_0 + \frac{\eta f_t b z}{\tan \beta} \tag{4}$$

As presented in Table 1, as the reduction coefficient in Eq. (4) decreases from 1 to 0.1, the predicted shear capacity decreases and the mean value of model error increases from 0.71 to 1.32. As the reduction coefficient is set as 0.4, the predicted results agree well with the test results (see Fig. 3). Accordingly,  $\eta = 0.4$  is recommended in Eq. (4). Unfortunately, the COV of model error is relatively high (i.e. 0.34), which is due to the fact that the proposed model is a semi-empirical form. Consequently, reliability analysis needs to be carried out for ensuring structural safety.

According to the unified standard for reliability design of building structures (GB 50068–2018) [38], the reduced design resistance  $R_d$  should be larger than the magnified design load effect  $S_d$ . For steel reinforced ECC beams, it can be expressed as

$$R_d(f_{tk}/\gamma_{ECC}, f_{yk}/\gamma_{steel} \dots) \geq S_d = \sum \gamma_i S_{ik} \tag{5}$$

where  $f_{tk}$  is the nominal value of the ultimate tensile strength of ECC.  $\gamma_{ECC}$  is the partial factor of ECC.  $f_{yk}$  is the nominal value of the yield strength of steel bars.  $\gamma_{steel}$  is the partial factor of steel bars, usually taken as  $\gamma_{steel} = 1.1$ .  $\gamma_i$  (such as  $\gamma_G$  and  $\gamma_Q$ ) is the partial factor of load effect, as described in Section 4.1.  $S_{ik}$  (such as  $S_{Gk}$  and  $S_{Qk}$ ) is the nominal value of load effect. The essence of Eq. (5) is to make structural safety level meet target reliability by a reduction factor (such as  $\gamma_{ECC}$ ) [34]. Therefore,  $\gamma_{ECC}$  will be calibrated in this study.

#### 4. Statistical characteristics of random variables

##### 4.1. Load effect

Resistance effect  $R$  and load effect  $S$  determine the reliability of structural members. According to GB 50068–2018 [38], load effect is expressed as

$$S = S_G + S_Q = \gamma_G S_{Gk} + \gamma_Q S_{Qk} \tag{6}$$

where  $S_G$  and  $S_Q$  are the dead load effect and live load effect, respectively.  $S_{Gk}$  and  $S_{Qk}$  are the nominal values of dead load and live load.  $\gamma_G$  and  $\gamma_Q$  are the partial factors of dead load and live load.  $\gamma_G = 1.3$  and  $\gamma_Q = 1.5$  are suggested in GB 50068–2018 [38]. Table 2 lists the statistical parameters and distribution types of load. Two live loads (i.e. house and office) will be considered in this study.

**Table 3**  
Statistical parameters and distribution types of material properties.

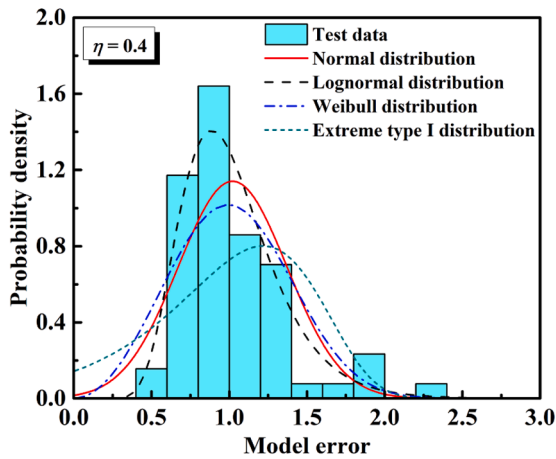
Material parameter	Bias	Coefficient of variation	Distribution type	Reference
Strength of steel bar (MPa)	1.156	0.0820	Normal distribution	[40]
Ultimate tensile strength of ECC (MPa)	1.115	0.0627	Normal distribution	[36]

**Table 4**  
Statistical parameters and distribution types of geometric parameters.

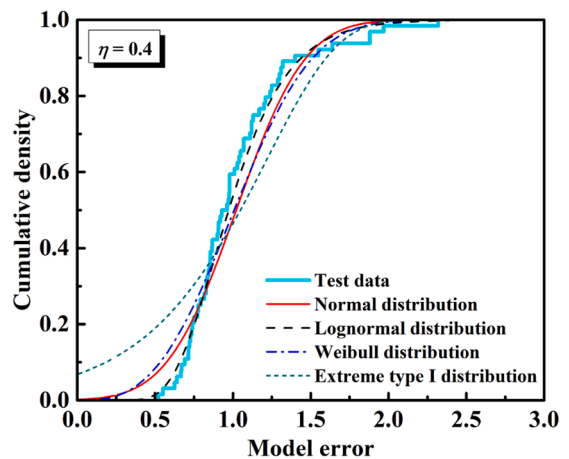
Geometric parameter	Bias	Coefficient of variation	Distribution type	Reference
Width (mm)	1.00	0.02	Normal distribution	[41]
Effective height (mm)	1.00	0.03	Normal distribution	[41]
Stirrup area (mm <sup>2</sup> )	1.00	0.03	Normal distribution	[41]
Stirrup space (mm)	0.99	0.07	Normal distribution	[41]

**Table 5**  
Kolmogorov-Smirnov testing result of model error ( $\eta = 0.4$ ).

Distribution type	Testing result	P-value
Normal distribution	1	$8.93 \times 10^{-29}$
Lognormal distribution	0	$7.12 \times 10^{-1}$
Weibull distribution	0	$2.30 \times 10^{-1}$
Extreme type I distribution	1	$5.89 \times 10^{-3}$



(a) Probability density function



(b) Cumulative density function

Fig. 4. Distribution type of model error.

4.2. Resistance effect

Resistance effect is determined by material properties, geometric parameters and calculation model. The uncertainties of material properties, geometric parameters and calculation model will be described below.

4.2.1. Uncertainty of material properties

The uncertainty of material properties is the differences of material properties in the structural members, which results from material quality and production process. The material properties include the tensile strength of steel bars and ECC. Table 3 lists the statistical parameters and distribution types of material properties.

4.2.2. Uncertainty of geometric parameters

The uncertainty of geometric parameters is the differences of the geometric dimension of member section, which results from manufacturing and installation. The geometric parameters include cross-section width, cross-section effective height, stirrup area and

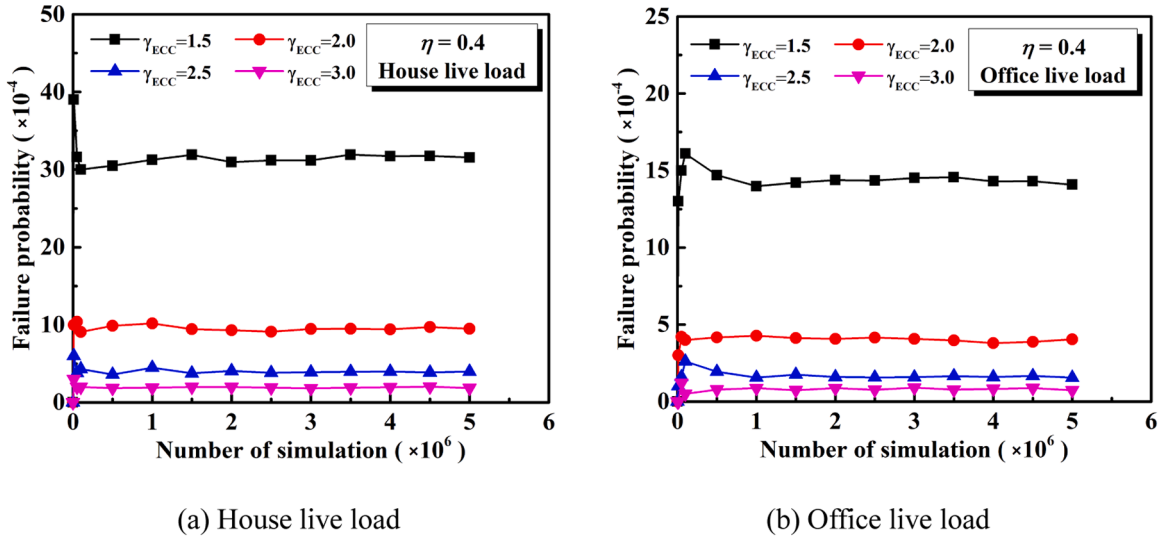


Fig. 5. Relationship between number of simulation and failure probability.

stirrup space. Table 4 lists the statistical parameters and distribution types of geometric parameters.

4.2.3. Uncertainty of calculation model

Hypothesis testing is carried out for determining the probability distribution of the model error in Section 3. Kolmogorov-Smirnov (K-S) testing is adopted in this research, and the corresponding significance level is set as 0.05. The hypothesis is accepted when testing result equals to zero; however, the hypothesis is rejected when testing result equals to one [34]. Table 5 and Fig. 4 present the testing results and distributions of the model error, respectively. Obviously, the model error follows the lognormal distribution.

5. Reliability analysis of steel reinforced ECC beams

5.1. Limit state function

The difference between resistance effect and load effect is limit state function Z, and it is expressed as

$$Z = R - S = \mu V_u - S_G - S_Q \tag{7}$$

Accordingly, the structural members are in reliable state ( $Z > 0$ ), limit state ( $Z = 0$ ) and failure state ( $Z < 0$ ). Based on the limit state (i.e.  $R_d = S_d$ ) and Eq. (6), the nominal values of dead load  $S_{Gk}$  and live load  $S_{Qk}$  are written as

$$S_{Gk} = \frac{R_d}{\gamma_G + \gamma_Q k} \tag{8}$$

$$S_{Qk} = \frac{R_d k}{\gamma_G + \gamma_Q k} \tag{9}$$

where  $k$  is the ratio of  $S_{Qk}$  and  $S_{Gk}$  (i.e. live-to-dead load ratio).

5.2. Monte Carlo simulation

Reliability index  $\beta$  can be calculated by Monte Carlo simulation [40,42]. As previously mentioned, it is considered as failure when Z is less than zero. If failure number in N simulations is n, the corresponding failure probability  $P_f$  can be given as

$$P_f = \frac{n}{N} \tag{10}$$

And reliability index can be given as

$$\beta = \Phi^{-1}(1 - P_f) \tag{11}$$

where  $\Phi^{-1}(\cdot)$  is the inverse standard normal distribution.

The calculation accuracy of Monte Carlo simulation depends on the number of simulation (i.e. N). When the number of simulation is very high, the calculated value is close to the true value [42]. Fig. 5 presents the relationship between number of simulation and

**Table 6**  
Design space of random variables.

Random variable	Value range	Number
Live-to-dead load ratio	0.5, 1.0, 1.5, 2.0, 2.5	5
Ultimate tensile strength of ECC (MPa)	3, 4, 5, 6, 7, 8	6
Strength grade of steel stirrup	HRB335, HRB400, HRB500	3
Width (mm)	100, 150, 200, 250, 300	5
Effective height (mm)	$0.8 \times 2b$	1
Stirrup area (mm <sup>2</sup> )	50, 100, 150	3
Stirrup space (mm)	150, 200, 250	3

Note: HRB335 is the steel bar with a yield strength nominal value of 335 MPa. Other steel identifiers have similar meanings.

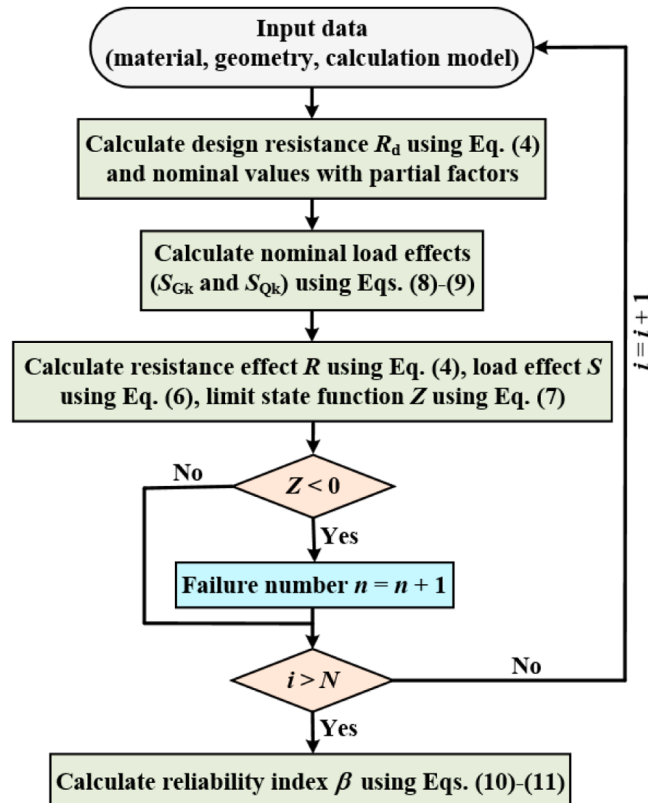


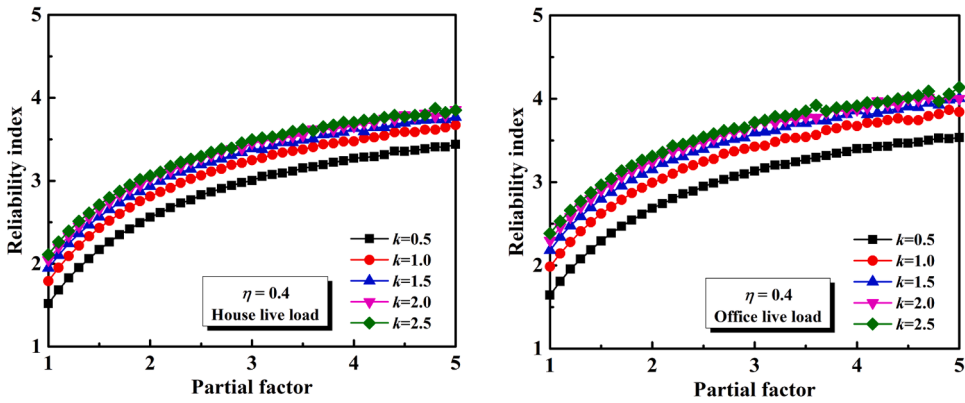
Fig. 6. Flowchart of reliability analysis.

failure probability. After  $2 \times 10^6$  times, failure probability almost does not change with the number of simulation. Therefore, the number of Monte Carlo simulation is set to be  $2 \times 10^6$ .

5.3. Design space and calculation flowchart

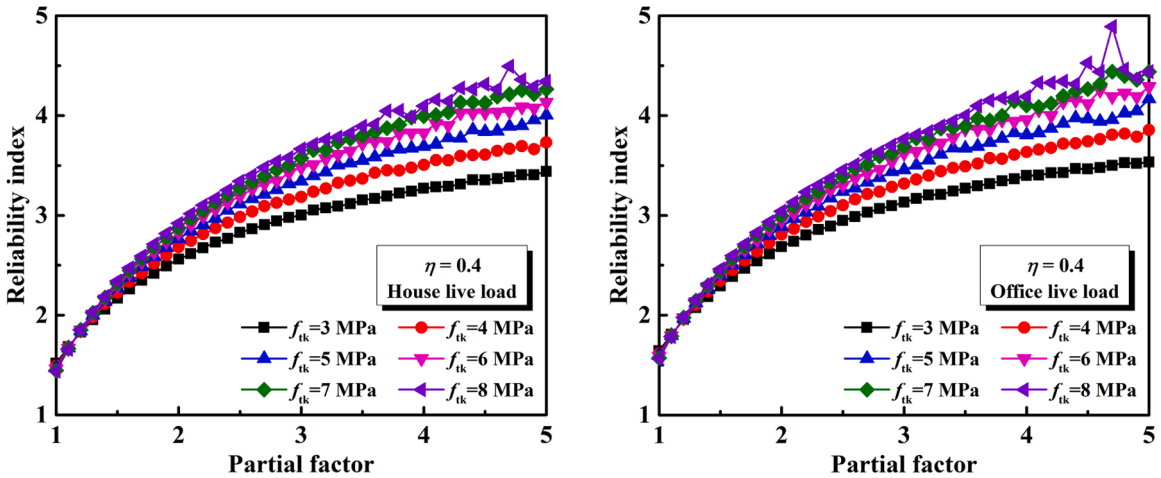
Table 6 lists the design space of random variables in reliability analysis. Five values are adopted (i.e. 0.5, 1.0, 1.5, 2.0 and 2.5) for analyzing the effects of the live-to-dead load ratio (i.e.  $k$ ) on reliability index [34]. The influences of ECC strength on the reliability index are analyzed, namely six strength grades [21–31,43–48]. Additionally, stirrup strength and geometric parameters are also considered in reliability analysis [21–31]. Consequently, the combination number of design variables in the whole design space is set as  $N_{ds} = 5 \times 6 \times 3 \times 5 \times 3 \times 3 = 4050$ . Since two live loads (house and office) are considered,  $4050 \times 2 = 8100$  reliability indexes needs to be calculated.

Fig. 6 presents the flowchart of reliability analysis. To obtain the nominal load effects, design resistance is calculated through using Eq. (4) ( $\eta = 0.4$ ) and nominal values with partial factors (i.e. material design strength). And then the nominal load effects are calculated based on Eqs. (8)–(9). Afterwards, the value of limit state function is determined by Eq. (4), Eq. (6) and Eq. (7). When the value is less than zero, it is considered as failure and failure number is increased by one. After  $N$  cycles, reliability index can be obtained through Eqs. (10)–(11).



(a) House live load (b) Office live load

Fig. 7. Effect of load effect ratio and partial factor on reliability index.



(a) House live load (b) Office live load

Fig. 8. Effect of ECC strength and partial factor on reliability index.

5.4. Results and discussion

5.4.1. Reliability index

The effect of load effect ratio (i.e.  $k$ ) and partial factor (i.e.  $\gamma_{ECC}$ ) on reliability index is shown in Fig. 7. Reliability index increases when load effect ratio increases from 0.5 to 2.5. A similar result can be found in the literature [34]. The result is due to the fact that live load has lower bias in comparison with dead load, as presented in Table 2. When the partial factor grows from 1 to 2.5, the design resistance  $R_d$  in Eqs. (8)–(9) decreases and then load effect reduces. It should be noted that resistance effect is not affected by the partial factor. As a result, reliability index increases as the partial factor is improved. Additionally, since house live load has higher bias in comparison with office live load, house live load is smaller than office live load in terms of reliability index.

Fig. 8 presents the influence of ECC strength and partial factor (i.e.  $\gamma_{ECC}$ ) on reliability index. Reliability index increases with the increment of ECC strength, especially at the high partial factor. The main reason for this result is as follows. As shown in Fig. 9, design resistance ratio (i.e.  $R_d(\gamma_{ECC} = 1 \dots) / R_d(\gamma_{ECC} = j \dots)$ ) decreases with the increase of ECC strength. According to Eqs. (8)–(9), the load effect  $S$  in Eq. (7) decreases with the ECC strength, especially at the high partial factor. It is noteworthy that the resistance effect  $R$  in Eq. (7) is not affected by the partial factor. On the other hand, reliability index fluctuates significantly with the partial factor, which is attributed to the fact that reliability index is very sensitive to the low failure probability [41].

Fig. 10 shows the influence of stirrup strength and partial factor (i.e.  $\gamma_{ECC}$ ) on reliability index. Reliability index reduces with the increment of stirrup strength, especially at the high partial factor. The main reason for this result is as follows. Design resistance ratio increases with the increment of stirrup strength, as presented in Fig. 11. According to Eqs. (8)–(9), the load effect in Eq. (7) increases with the stirrup strength. And the partial factor has no effect on the resistance effect in Eq. (7).

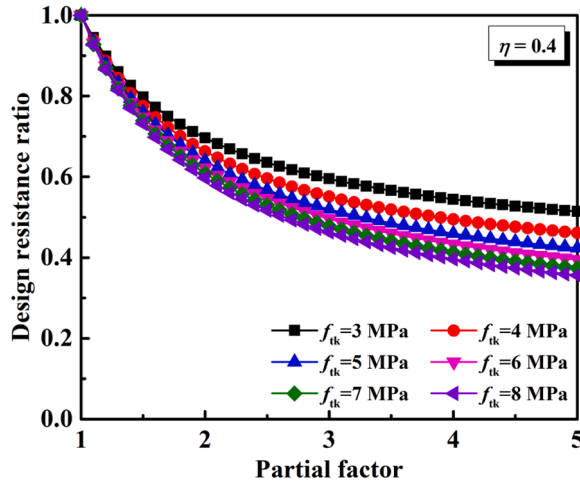


Fig. 9. Influence of ECC strength and partial factor on design resistance ratio.

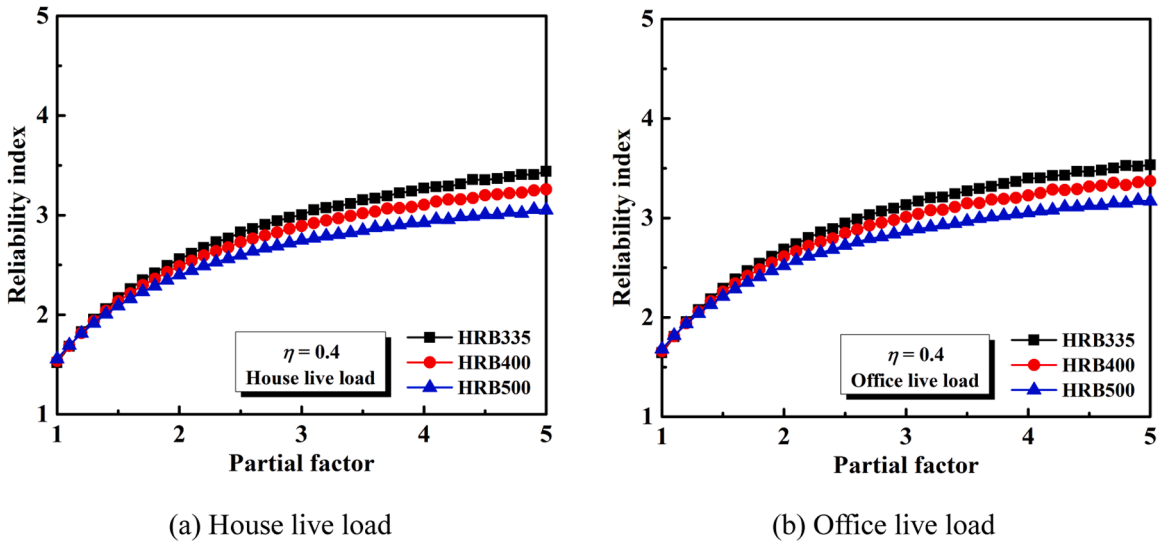


Fig. 10. Influence of stirrup strength and partial factor on reliability index.

Fig. 12 presents the influence of stirrup ratio (i.e.  $\rho_{sv} = \frac{A_{sv}}{A_b}$ ) and partial factor (i.e.  $\gamma_{ECC}$ ) on reliability index. Reliability index obviously reduces as stirrup ratio is increased, especially at the high partial factor. Design resistance ratio obviously increases with the increment of stirrup ratio, as displayed in Fig. 13. According to Eqs. (8)–(9), the load effect in Eq. (7) obviously increases with the stirrup ratio. In Fig. 12, reliability index obviously fluctuates with the partial factor, which may be due to the fact that reliability index is very sensitive to the low failure probability.

5.4.2. Calibration for partial factor

To obtain the recommended value of partial factor  $\gamma_{ECC}$ , a calibration process is necessary. According to the literature [34,42], a least-square formula is introduced for computing the deviation  $H$  between the calculated reliability index  $\beta_i$  and target reliability index  $\beta_T$ . It is expressed as

$$H = \frac{1}{N_{ds}} \sum_{i=1}^{N_{ds}} (\beta_i - \beta_T)^2 \tag{12}$$

As listed in Table 7, the target reliability index in GB 50068–2018 [38] is determined based on safety level and failure mode. Accordingly, four target reliability indexes (i.e. 2.7, 3.2, 3.7 and 4.2) will be considered in this study.

Fig. 14 shows the average deviation from target reliability index. The partial factor at minimum average deviation is the recommended value of partial factor  $\gamma_{ECC}$ . For different target reliability indexes, the recommended value is listed in Table 8. House live load

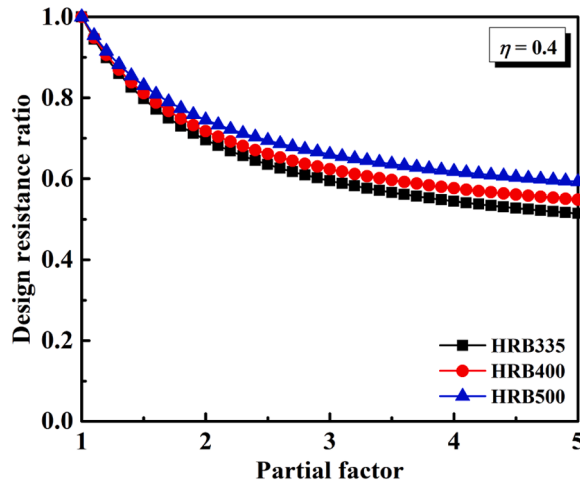


Fig. 11. Effect of stirrup strength and partial factor on design resistance ratio.

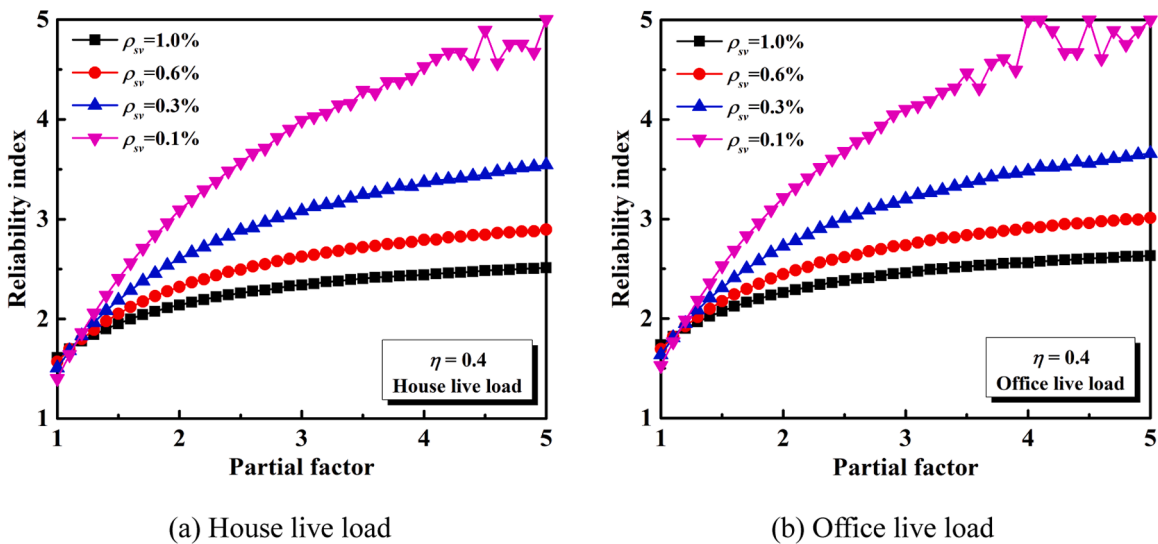


Fig. 12. Effect of stirrup ratio and partial factor on reliability index.

possesses higher partial factor when compared with office live load. It is noted that the literature [34] has a similar result. Besides, with the increase of target reliability index, the recommended value of partial factor increases.

The recommended values of the partial factors listed in Table 8 are relatively high, which is due to the high COV of model error (i.e. 0.34). As shown in Fig. 15, when the partial factor  $\gamma_{ECC}$  is constant, reliability index reduces significantly with the increasing COV of model error. Similarly, the recommended partial factor of fiber reinforced polymer/plastic (FRP) in the literature [49] is higher than that in GB 50608–2020 [50], which is attributed to the high COV of model error (i.e. 0.335–0.426). On the other hand, it is also due to the difference in characterizing strength of ECC between the present article and those codes [36,51]. More importantly, the values of the partial factors in Table 8 seem relatively high, but in principle consistent with those recommended in the current codes [36,51]. In the current codes, such as [51], the tensile strength value used to calculate the flexural strength of ECC structures with a reliability of 3.2 is exactly a design value of tensile yield strength, as displayed in Fig. 16. It is known that under increasing tension, ECC similar to steel bar experiences three different stages, i.e. elastic stage, strain-hardening stage and failure stage. In attempt to obtain the value of ECC for structural design, several special factors are introduced to derive different tensile strength, which are the nominal value of the ultimate tensile strength, the nominal value of the tensile yield strength, and the design value of the tensile yield strength in order. According to [51], the gap between the ultimate tensile strength and design value can be characterized by a triple product from  $\gamma_1 = 1.3$ ,  $\gamma_2 = 1.25$  and  $\gamma_3 = 1.3$ , and at last it turns out to be a constant of 2.1. Compared with the constant, the recommended partial factors in this study show more concerns about the variation of reliability and load category.

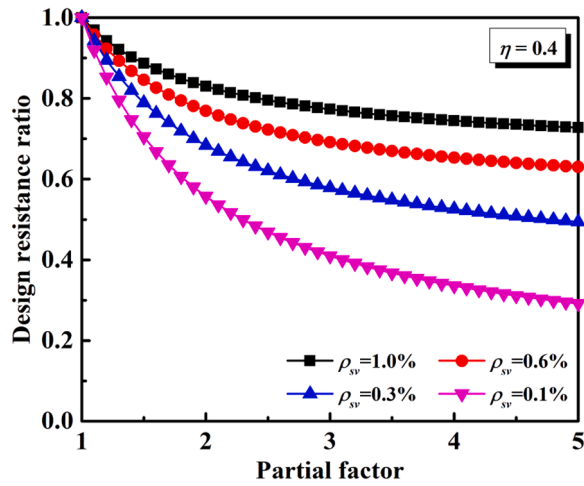


Fig. 13. Effect of stirrup ratio and partial factor on design resistance ratio.

Table 7  
Target reliability index under ultimate limit state [38].

Failure mode	Safety level		
	First level	Second level	Third level
Ductile failure	3.7	3.2	2.7
Brittle failure	4.2	3.7	3.2

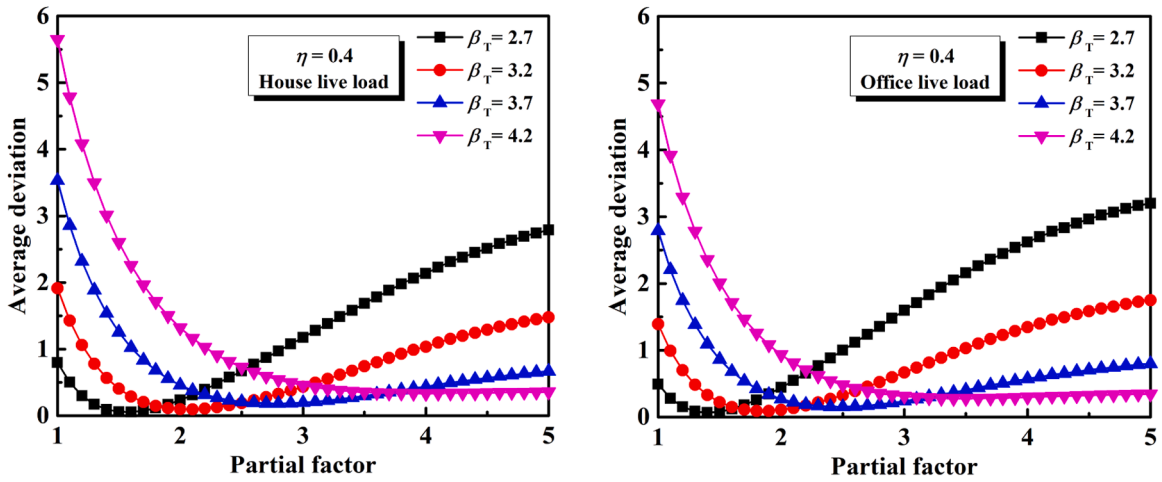


Fig. 14. Average deviation from target reliability index.

Table 8  
Recommended value of partial factor.

Live load type	Recommended value of partial factor $\gamma_{ECC}$			
	$\beta_T = 2.7$	$\beta_T = 3.2$	$\beta_T = 3.7$	$\beta_T = 4.2$
House live load	1.6	2.1	2.8	4.0
Office live load	1.4	1.8	2.5	3.5

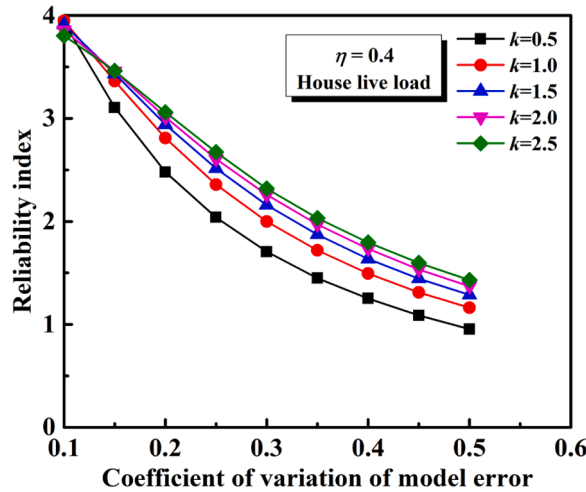


Fig. 15. Relationship between reliability index and the coefficient of variation of model error.

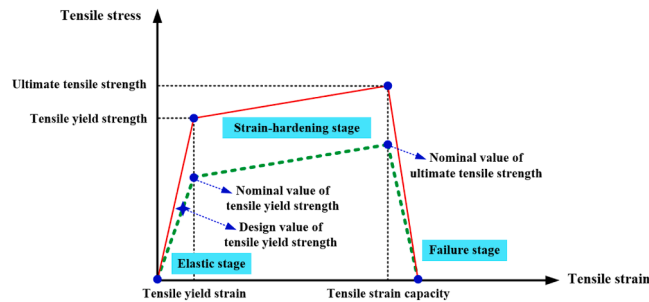


Fig. 16. Stress-strain relationship of ECC under tension.

6. Conclusions

In this research, a test database of steel reinforced ECC beams under shear loading was constructed. The simplified shear capacity model of steel reinforced ECC beams was preliminary established. The statistical characteristics related to random variables were described and determined, and reliability index was investigated through Monte Carlo simulation. Afterwards, the reliability-based shear capacity design model of steel reinforced ECC beams was established. The critical conclusions can be drawn:

- 1) According to GB 50010–2010 [33] and considering the shear resistance provided by fibers, the simplified shear capacity model of steel reinforced ECC beams is preliminary established. As reduction coefficient is 0.4 in the proposed shear capacity model, the predicted results agree well with the test results. Kolmogorov-Smirnov testing indicates that model error follows the lognormal distribution.
- 2) House live load is smaller than office live load in terms of reliability index. When load effect ratio or the partial factor of ECC increases, reliability index increases. Reliability index also increases with the increase of ECC strength, especially at the high partial factor. On the contrary, reliability index reduces with the increment of stirrup strength or stirrup ratio, especially at the high partial factor.
- 3) As target reliability index is improved, the recommended partial factor of ECC increases. House live load possesses high partial factor in comparison with office live load. The recommended partial factors corresponding to the various target reliability indexes required by Chinese code are illustrated in Table 8, which is an important basis for the reliability-based shear capacity model.

Declaration of Competing Interest

The authors declare that they have no known competing financial interests or personal relationships that could have appeared to influence the work reported in this paper.

## Data Availability

Data has been provided in Appendix.

## Acknowledgement

The authors gratefully acknowledge the financial support by the National Natural Science Foundation of China (No. 51978504).

## Appendix A

**Table A**

Details of steel reinforced ECC beams in test database.

Beam ID	Cross section (mm)	Shear-span ratio	$f_c$ (MPa)	$f_t$ (MPa)	$f_{yv}$ (MPa)	$A_{sv}$ (mm <sup>2</sup> )	$s$ (mm)	$V_{uc}$ (kN)	Reference
RE-00	300 × 150	2.80	32.80	3.71	–	–	–	104.38	[21]
RE-12	300 × 150	2.80	35.60	3.68	323.00	63.31	352	126.05	
RE-24	300 × 150	2.80	31.50	3.39	323.00	63.31	176	125.24	
RE-30	300 × 150	2.80	33.10	3.56	323.00	63.31	141	130.56	
RE-42	300 × 150	2.80	30.40	3.67	323.00	63.31	100	141.09	
X1	200 × 120	2.00	45.20	2.34	–	–	–	41.20	[22]
X2	200 × 120	2.00	53.00	3.26	–	–	–	68.20	
X3	200 × 120	2.00	53.80	3.96	–	–	–	70.70	
X4	200 × 120	2.00	60.90	4.97	–	–	–	95.20	
X5	200 × 120	2.00	62.00	5.89	–	–	–	111.65	
J4	200 × 120	2.50	60.90	4.97	–	–	–	87.70	
J5	200 × 120	3.00	60.90	4.97	–	–	–	73.15	
J6	200 × 120	3.50	60.90	4.97	–	–	–	64.15	
Z1	200 × 120	2.00	60.90	4.97	–	–	–	85.20	
G1	200 × 120	2.00	60.90	4.97	477.50	57.00	120	149.15	
G2	200 × 120	2.00	60.90	4.97	477.50	57.00	140	131.20	
G3	200 × 120	2.00	60.90	4.97	477.50	57.00	160	127.70	
G4	200 × 120	2.00	60.90	4.97	477.50	57.00	180	124.65	
G5	200 × 120	2.00	60.90	4.97	477.50	57.00	200	120.20	
G6	200 × 120	2.00	60.90	4.97	477.50	57.00	230	110.70	
G7	200 × 120	2.00	60.90	4.97	477.50	57.00	260	107.70	
Df	180 × 120	3.06	46.22	4.33	–	–	–	58.39	[23]
Ef	180 × 120	3.08	46.39	4.33	–	–	–	66.60	
SE-2a	180 × 120	2.00	70.55	5.83	392.00	57.00	80	285.00	[24]
SE-2	180 × 120	2.00	70.55	5.83	392.00	57.00	60	326.00	
SE-2c	180 × 120	2.00	70.55	5.83	392.00	57.00	80	352.00	
D-U2	180 × 120	2.04	46.22	4.30	–	–	–	85.10	[25]
D-U3	180 × 120	3.06	46.22	4.30	–	–	–	58.39	
D-U4	180 × 120	4.08	46.59	4.30	–	–	–	43.77	
E-U2	180 × 120	2.06	46.59	4.30	–	–	–	95.86	
E-U3	180 × 120	3.08	45.73	4.30	–	–	–	66.60	
E-U4	180 × 120	4.11	45.73	4.30	–	–	–	50.61	
F-U2	180 × 120	2.01	47.76	4.30	–	–	–	103.94	
F-U3	180 × 120	3.02	47.76	4.30	–	–	–	70.03	
F-U4	180 × 120	4.03	47.76	4.30	–	–	–	62.67	
E-N	400 × 200	2.50	56.40	8.00	–	–	–	289.50	[26]
E-S	400 × 200	2.50	54.70	7.50	440.00	190.20	250	421.40	
R/ECC-0	250 × 125	1.42	53.60	4.50	–	–	–	150.00	[27]
R/ECC-d	250 × 125	1.42	53.60	4.50	550.00	57.00	200	179.00	
R/ECC-1/2d	250 × 125	1.42	53.60	4.50	550.00	57.00	100	200.00	
R/ECC-1/4d	250 × 125	1.42	53.60	4.50	550.00	57.00	50	234.00	
PVA10-00	280 × 180	1.50	37.30	2.52	–	–	–	123.90	[28]
PVA10-15	280 × 180	1.50	37.30	2.52	294.50	25.12	93	144.80	
PVA10-30	280 × 180	1.50	37.30	2.52	294.50	25.12	47	171.50	
PVA15-00	280 × 180	1.50	35.70	2.50	–	–	–	142.80	
PVA15-15	280 × 180	1.50	35.70	2.50	294.50	25.12	93	169.70	
PVA15-30	280 × 180	1.50	35.70	2.50	294.50	25.12	47	182.90	
PVA20-00	280 × 180	1.50	39.10	4.06	–	–	–	182.70	
PVA20-15	280 × 180	1.50	39.10	4.06	294.50	25.12	93	205.80	
PVA20-30	280 × 180	1.50	39.10	4.06	294.50	25.12	47	208.60	
E-25	180 × 120	2.50	70.55	5.83	–	–	–	209.85	[29]
E-3	180 × 120	3.00	70.55	5.83	–	–	–	173.25	
A2	180 × 120	3.00	71.00	3.92	–	–	–	98.25	[30]
A3	180 × 120	3.00	60.16	4.58	–	–	–	143.55	

(continued on next page)

Table A (continued)

Beam ID	Cross section (mm)	Shear-span ratio	$f_c$ (MPa)	$f_t$ (MPa)	$f_{yv}$ (MPa)	$A_{sv}$ (mm <sup>2</sup> )	$s$ (mm)	$V_{uc}$ (kN)	Reference
A4	180 × 120	3.00	71.29	6.00	–	–	–	160.10	
A5	180 × 120	3.00	70.55	7.30	–	–	–	173.25	
B5	180 × 120	4.00	70.55	7.30	–	–	–	154.80	
B6	180 × 120	4.00	70.55	7.30	–	–	–	136.65	
EU-S0	180 × 120	3.08	45.73	4.38	–	–	–	66.60	[31]
EU-S3	180 × 120	3.08	45.73	4.38	316.00	66.33	225	70.55	
EU-S6	180 × 120	3.08	45.73	4.38	316.00	66.33	150	67.62	
FU-S0	180 × 120	3.02	47.76	4.38	–	–	–	70.03	
FU-S3	180 × 120	3.02	47.76	4.38	316.00	66.33	225	78.25	
FU-S6	180 × 120	3.02	47.76	4.38	316.00	66.33	150	71.20	

Note:  $f_c$  is the compressive strength of ECC.

## References

- [1] V.C. Li, D.K. Mishra, H.C. Wu, Matrix design for pseudo-strain-hardening fibre reinforced cementitious composites, *Mater. Struct.* 28 (184) (1995) 586–595, <https://doi.org/10.1007/BF02473191>.
- [2] K.Q. Yu, M.F. Lin, L.K. Tian, Y. Ding, Long-term stable and sustainable high-strength engineered cementitious composite incorporating limestone powder, *Structures* 47 (2023) 530–543, <https://doi.org/10.1016/j.istruc.2022.10.008>.
- [3] B.Y. Deng, D. Tan, L.Z. Li, Z. Zhang, Z.W. Cai, K.Q. Yu, Flexural behavior of precast ultra-lightweight ECC-concrete composite slab with lattice girders, *Eng. Struct.* 279 (2023), 115553, <https://doi.org/10.1016/j.engstruct.2022.115553>.
- [4] Z.G. Zhang, Q. Zhang, Matrix tailoring of engineered cementitious composites (ECC) with non-oil-coated, low tensile strength PVA fiber, *Constr. Build. Mater.* 161 (2018) 420–431, <https://doi.org/10.1016/j.conbuildmat.2017.11.072>.
- [5] H. Zhu, D. Zhang, T.Y. Wang, H.L. Wu, V.C. Li, Mechanical and self-healing behavior of low carbon engineered cementitious composites reinforced with PP-fibers, *Constr. Build. Mater.* 259 (2020), 119805, <https://doi.org/10.1016/j.conbuildmat.2020.119805>.
- [6] Z.G. Zhang, Y.Z. Ding, S.Z. Qian, Influence of bacterial incorporation on mechanical properties of engineered cementitious composites (ECC), *Constr. Build. Mater.* 196 (2019) 195–203, <https://doi.org/10.1016/j.conbuildmat.2018.11.089>.
- [7] Q. Liao, L.Z. Li, B.X. Li, J.T. Yu, Prediction on the flexural deflection of ultra-high strength rebar reinforced ECC beams at service loads, *Structures* 33 (2021) 246–258, <https://doi.org/10.1016/j.istruc.2021.04.050>.
- [8] K.Q. Yu, W. Mcgee, T.Y. Ng, H. Zhu, V.C. Li, 3D-printable engineered cementitious composites (3DP-ECC): fresh and hardened properties, *Cem. Concr. Res.* 143 (2021), 106388, <https://doi.org/10.1016/j.cemconres.2021.106388>.
- [9] E.H. Yang, S. Wang, Y. Yang, V.C. Li, Fiber-bridging constitutive law of engineered cementitious composites, *J. Adv. Concr. Technol.* 6 (1) (2008) 181–193, <https://doi.org/10.3151/jact.6.181>.
- [10] Q. Liao, J.T. Yu, X.X. Xie, J.H. Ye, F.M. Jiang, Experimental study of reinforced UHPC panels under close-in blast loading, *J. Build. Eng.* 46 (2022), 103498, <https://doi.org/10.1016/j.job.2021.103498>.
- [11] Y.C. Wang, F.C. Liu, J.T. Yu, F.Y. Dong, J.H. Ye, Effect of polyethylene fiber content on physical and mechanical properties of engineered cementitious composites, *Constr. Build. Mater.* 251 (2020), 118917, <https://doi.org/10.1016/j.conbuildmat.2020.118917>.
- [12] Z.F. Dong, H.L. Tan, J.T. Yu, F.C. Liu, A feasibility study on engineered cementitious composites mixed with coarse aggregate, *Constr. Build. Mater.* 350 (2022), 128587, <https://doi.org/10.1016/j.conbuildmat.2022.128587>.
- [13] J.H. Ye, C. Cui, J.T. Yu, K.Q. Yu, J.Z. Xiao, Fresh and anisotropic-mechanical properties of 3D printable ultra-high ductile concrete with crumb rubber, *Compos. Pt B-Eng.* 211 (2021), 108639, <https://doi.org/10.1016/j.compositesb.2021.108639>.
- [14] K.Q. Yu, Y.C. Wang, J.T. Yu, S.L. Xu, A strain-hardening cementitious composites with the tensile capacity up to 8, *Constr. Build. Mater.* 137 (2017) 410–419, <https://doi.org/10.1016/j.conbuildmat.2017.01.060>.
- [15] Z.G. Zhang, F. Yang, J.C. Liu, S.P. Wang, Eco-friendly high strength, high ductility engineered cementitious composites (ECC) with substitution of fly ash by rice husk ash, *Cem. Concr. Res.* 137 (2020), 106200, <https://doi.org/10.1016/j.cemconres.2020.106200>.
- [16] N. Xu, Y. Qian, J. Yu, C.K.Y. Leung, Tensile performance of 3D-printed strain-hardening cementitious composites (SHCC) considering material parameters, nozzle size and printing pattern, *Cem. Concr. Compos.* 132 (2022), 104601, <https://doi.org/10.1016/j.cemconcomp.2022.104601>.
- [17] K.Q. Yu, H. Zhu, M.J. Hou, V.C. Li, Self-healing of PE-fiber reinforced lightweight high-strength engineered cementitious composite, *Cem. Concr. Compos.* 123 (2021), 104209, <https://doi.org/10.1016/j.cemconcomp.2021.104209>.
- [18] Q. Liao, J.T. Yu, T.C. Shi, Y.R. Su, Mechanical behaviors and failure criteria of seawater sea-sand engineered cementitious composites under combined tension and shear, *J. Build. Eng.* 54 (2022), 104552, <https://doi.org/10.1016/j.job.2022.104552>.
- [19] Z.H. Guo, X.D. Shi, *Reinforced Concrete Theory and Analyse*, Tsinghua University Press, Beijing, China, 2003.
- [20] Q. Liao, Y.R. Su, J.T. Yu, K.Q. Yu, Compression-shear performance and failure criteria of seawater sea-sand engineered cementitious composites with polyethylene fibers, *Constr. Build. Mater.* 345 (2022), 128386, <https://doi.org/10.1016/j.conbuildmat.2022.128386>.
- [21] R. Zhang, Q.L. Meng, W. He, J. Niwa, Experimental investigation on shear behavior of PP-ECC beams by considering effect of stirrup, *China J. Highw. Transp.* 30 (12) (2017) 234–241.
- [22] Y.Q. Wang, L. Sun, Y.M. Gao, S.G. Liu, Experimental study on shear performance of oblique section of PVA-ECC beams, *Industrial, Construction* 49 (1) (2019) 184–188.
- [23] S.L. Xu, L.J. Hou, X.F. Zhang, Flexural and shear behaviors of reinforced ultrahigh toughness cementitious composite beams without web reinforcement under concentrated load, *Eng. Struct.* 39 (2012) 176–186, <https://doi.org/10.1016/j.engstruct.2012.01.011>.
- [24] X.S. Li, J. Dai, M.K. Deng, Shear behavior of high ductile fiber reinforced concrete beams, *Alex. Eng. J.* 60 (2021) 1665–1675, <https://doi.org/10.1016/j.aej.2020.11.017>.
- [25] S.L. Xu, L.J. Hou, X.F. Zhang, Shear behavior of reinforced ultrahigh toughness cementitious composite beams without transverse reinforcement, *J. Mater. Civ. Eng.* 24 (10) (2012) 1283–1294, [https://doi.org/10.1061/\(ASCE\)MT.1943-5533.0000505](https://doi.org/10.1061/(ASCE)MT.1943-5533.0000505).
- [26] D.W. Gu, J.L. Pan, S. Mustafa, Y.T. Huang, M. Lukovi, Shear transfer mechanism in reinforced engineered cementitious composite (ECC) beams: quantification of  $V_s$  and  $V_c$ , *Eng. Struct.* 261 (2022), 114282, <https://doi.org/10.1016/j.engstruct.2022.114282>.
- [27] I. Paegle, G. Fischer, Phenomenological interpretation of the shear behavior of reinforced engineered cementitious composite beams, *Cem. Concr. Compos.* 73 (2016) 213–225, <https://doi.org/10.1016/j.cemconcomp.2016.07.018>.
- [28] Shimizu K., Kanakubo T., Kanda T., Nagai S. Shear behavior of steel reinforced PVA-ECC beams. In Proceedings of the 13th World Conference on Earthquake Engineering, Vancouver, BC, Canada, 2004.
- [29] M.K. Deng, J. Dai, X.W. Liang, M.Y. Zhang, Experimental study on the shear behavior of high ductile fiber reinforced concrete beams without stirrups, *Eng. Mech.* 33 (17) (2016) 208–216.

- [30] J. Dai, M.K. Deng, J.L. Chen, Influence of matrix ductility on shear behavior of high ductile fiber reinforced concrete beams, *Eng. Mech.* 35 (2) (2018) 124–132.
- [31] L.J. Hou, S.L. Xu, X.F. Zhang, D. Chen, Shear behaviors of reinforced ultrahigh toughness cementitious composite slender beams with stirrups, *J. Mater. Civ. Eng.* 26 (3) (2014) 466–475, [https://doi.org/10.1061/\(ASCE\)MT.1943-5533.0000833](https://doi.org/10.1061/(ASCE)MT.1943-5533.0000833).
- [32] Z. Qiao, Z.F. Pan, C.K.Y. Leung, S.P. Meng, Calculation method for shear strength of reinforced ECC beams using modified compression field theory, *J. Southeast Univ. (Nat. Sci. Ed.)* 48 (6) (2018) 1021–1027.
- [33] GB 50010-2010, Code for Design of Concrete Structures, China Architecture and Building Press, Beijing, 2010.
- [34] X.X. Huang, L.L. Sui, F. Xing, Y.W. Zhou, Y.F. Wu, Reliability assessment for flexural FRP-strengthened reinforced concrete beams based on importance sampling, *Compos. Pt B-Eng.* 156 (2) (2019) 378–398, <https://doi.org/10.1016/j.compositesb.2018.09.002>.
- [35] Q. Liao, Y.R. Su, J.T. Yu, K.Q. Yu, Torsional behavior of BFRP bars reinforced engineered cementitious composites beams without stirrup, *Eng. Struct.* 268 (1) (2022), 114748, <https://doi.org/10.1016/j.engstruct.2022.114748>.
- [36] JSCE, Recommendations for design and construction of high performance fiber reinforced cement composites with multiple fine cracks. Japan Society of Civil Engineers, Tokyo, 2008.
- [37] R. Park, T. Paulay, Reinforced Concrete Structures, John Wiley and Sons, New York, USA, 1975.
- [38] GB 50068-2018, Unified Standard for Reliability Design of Building Structures, China Architecture and Building Press, Beijing, 2018.
- [39] GB 50009-2012, Load Code for the Design of Building Structures, China Architecture and Building Press, Beijing, 2012.
- [40] J.L. Zhou, C.X. Li, Z.Y. Chen, Z. Feng, C.L. Fang, Y.B. Yan, Reliability analysis of torsional capacity of reinforced ultra-high performance concrete beams and determination of partial factor for materials, *China Civ. Eng. J.* 55 (2) (2022) 11–22.
- [41] G.Q. Li, H.W. Huang, X. Wu, S.R. Liu, Load and Reliability of Engineering Structures Design Principles, China Architecture and Building Press, Beijing, 2005.
- [42] F. Peng, W.C. Xue, Reliability-based design method for ultimate load-bearing capacity of GFRP reinforced concrete beams under flexure, *China Civ. Eng. J.* 51 (5) (2018) 60–67.
- [43] S.G. Liu, S. Lu, L.Q. Yin, C.W. Yan, L.H. Lu, J. Zhou, Mechanical strength model of engineered cementitious composites with freeze-thaw damage based on pore structure evolution, *Cem. Concr. Compos.* 134 (2022), 104706, <https://doi.org/10.1016/j.cemconcomp.2022.104706>.
- [44] J.S. Han, J.M. Cai, Y.Z. Lin, Y.Q. Sun, J.L. Pan, Impact resistance of engineered geopolymer composite (EGC) in cold temperatures, *Constr. Build. Mater.* 343 (2022), 128150, <https://doi.org/10.1016/j.conbuildmat.2022.128150>.
- [45] M.Z. Zhu, B. Chen, M. Wu, J.X. Han, Effects of different mixing ratio parameters on mechanical properties of cost-effective green engineered cementitious composites (ECC), *Constr. Build. Mater.* 328 (2022), 127093, <https://doi.org/10.1016/j.conbuildmat.2022.127093>.
- [46] G.A. Arce, H. Noorvand, M.M. Hassan, T. Rupnow, N. Dhakal, Feasibility of low fiber content PVA-ECC for jointless pavement application, *Constr. Build. Mater.* 268 (2021), 121131, <https://doi.org/10.1016/j.conbuildmat.2020.121131>.
- [47] C. Wu, V.C. Li, CFRP-ECC hybrid for strengthening of the concrete structures, *Compos. Struct.* 178 (2017) 372–382, <https://doi.org/10.1016/j.compstruct.2017.07.034>.
- [48] J. Yu, Y.W. Weng, J.T. Yu, W.G. Chen, S.N. Lu, K.Q. Yu, Generative AI for performance-based design of engineered cementitious composite, *Compos. Pt. B-Eng.* 266 (2023) 110993, <https://doi.org/10.1016/j.compositesb.2023.110993>.
- [49] Y.W. Zhou, J.X. Zhang, W.W. Li, B. Hu, X.X. Huang, Reliability-based design analysis of FRP shear strengthened reinforced concrete beams considering different FRP configurations, *Compos. Struct.* 237 (2020), 111957, <https://doi.org/10.1016/j.compstruct.2020.111957>.
- [50] GB 50608-2020, Technical Code for Infrastructure Application of FRP Composites, China Metallurgical Construction Association, Beijing, 2020.
- [51] DB/T 1937-2022, Technical Standard for Strengthening Masonry Structure with Engineered Cementitious Composites, China Architecture and Building Press, Beijing, 2022.